

Persisting quantum effects in the anisotropic Rabi model at thermal equilibrium

He-Guang Xu,¹ V. Montenegro,^{2,3,*} Gao Xianlong^{4,†}, Jiasen Jin^{1,‡} and G. D. de Moraes Neto^{4,§}

¹*School of Physics, Dalian University of Technology, 116024 Dalian, People's Republic of China*

²*Institute of Fundamental and Frontier Sciences, University of Electronic Science and Technology of China, Chengdu 611731, People's Republic of China*

³*Key Laboratory of Quantum Physics and Photonic Quantum Information, Ministry of Education, University of Electronic Science and Technology of China, Chengdu 611731, People's Republic of China*

⁴*Department of Physics, Zhejiang Normal University, Jinhua 321004, Zhejiang, People's Republic of China*



(Received 12 September 2023; accepted 6 December 2023; published 2 January 2024)

Quantum correlations and nonclassical states are at the heart of emerging quantum technologies. Efforts to produce long-lived states of such quantum resources are a subject of tireless pursuit. Among several platforms useful for quantum technology, the mature quantum system of light-matter interactions offers unprecedented advantages due to current on-chip nanofabrication, efficient quantum control of its constituents, and its wide range of operational regimes. Recently, a continuous transition between the Jaynes-Cummings model and the Rabi model has been proposed by exploiting anisotropies in their light-matter interactions, known as the anisotropic quantum Rabi model. In this paper, we study the long-lived quantum correlations and nonclassical states generated in the anisotropic Rabi model and how these indeed persist even at thermal equilibrium. To achieve this, we thoroughly analyze several quantumness quantifiers, where the long-lived quantum state is obtained from a dressed master equation that is valid for all coupling regimes and with the steady state ensured to be the canonical Gibbs state. Furthermore, we demonstrate a stark distinction between virtual excitations produced beyond the strong coupling regime and the quantumness quantifiers once the light-matter interaction has been switched off. This raises the key question about the nature of the equilibrium quantum features generated in the anisotropic quantum Rabi model and paves the way for future experimental investigations, without the need for challenging ground-state cooling.

DOI: [10.1103/PhysRevResearch.6.013001](https://doi.org/10.1103/PhysRevResearch.6.013001)

I. INTRODUCTION

The resource theory of quantum information [1,2] demonstrates that quantum correlations found in nonclassical states are of utmost importance for performing quantum processing tasks [3,4]. From a theoretical perspective, nonclassical states have proven highly valuable in investigating decoherence [5], witnessing the potential quantum nature of gravity [6,7], studying the quantum-to-classical transition [8], enabling remote quantum control of the weak value amplification [9], and serving as a powerful tool for witnessing quantum phase transitions in critical systems [10]. From a practical standpoint, quantum correlations have demonstrated their pivotal role as a fundamental element in emerging quantum technologies [11,12], including secure quantum communication

[13,14], quantum sensing [15–21], and quantum simulation [22]. Nonetheless, the intrinsic sources of noise and decoherence inherent in quantum dynamics render the production of long-lived quantum states necessary for quantum technologies [23,24]. Efforts to advance efficient techniques for generating and protecting nonclassical states against quantum noise [25] encompass approaches such as decoherence-free subspaces [26–28], dynamical decoupling [29,30], and reservoir engineering schemes [31–33]. Therefore, proposing schemes that facilitate the generation of long-lived highly correlated nonclassical states is one of the primary tasks within the quantum information field.

Quantum systems undergoing light-matter interactions stand as diverse platforms for generating nonclassical states and executing quantum information tasks [34,35]. The recently achieved ultrastrong coupling (USC) regime [36–38] and deep strong coupling (DSC) regime [39,40] of light-matter interactions have advanced quantum correlation generation beyond the strong coupling (SC) regime [41–45], i.e., when the light-matter coupling strength exceeds both the decay rates and the natural frequencies of the systems. Notably, a clear distinction between the USC and DSC regimes and the SC regime is the emergence of nonclassicality in the ground state of the system, manifested through squeezing and entanglement [46,47]. Moreover, within the USC regime, thermal photons can exhibit antibunching behavior [48], and

*vmontenegro@uestc.edu.cn

†gaoxl@zjnu.edu.cn

‡jsjin@dlut.edu.cn

§gdmneto@zjnu.edu.cn

Published by the American Physical Society under the terms of the [Creative Commons Attribution 4.0 International](https://creativecommons.org/licenses/by/4.0/) license. Further distribution of this work must maintain attribution to the author(s) and the published article's title, journal citation, and DOI.

emissions from the matter subsystem (e.g., a two-level atom) can display photon bunching [49], whereas the behavior is reversed in the SC regime.

The cornerstone model describing light-matter interaction is composed of a two-level atom (qubit) coupled to a quantized single-mode cavity field through dipole interaction, known as the quantum Rabi model (QRM) [50–52]. The QRM has been the subject of extensive theoretical work in quantum optics [53], for the generation of quantum entanglement [54], as an Otto quantum engine in quantum thermodynamics [55], and to exhibit the emergence of quantum phase transitions [56–58], and it motivated the development of a novel operational criterion for integrability [59,60]. Interestingly, the QRM transforms into the Jaynes-Cummings model (JCM) [61] in situations where the natural frequencies of the system significantly surpass the bare light-matter coupling strength. In this scenario, one can invoke the rotating-wave approximation (RWA), permitting the retention of the rotating-wave (RW) terms while omitting the counter-rotating-wave (CRW) terms. However, this approximation becomes invalid once the system transit towards the USC regime [60,62–65].

This motivates the introduction of a continuous transition between the JCM and the QRM by varying the RW and CRW coupling strengths, known as the anisotropic quantum Rabi model (AQRM). The AQRM has been explored in both closed systems [66,67] and open systems [68,69], with novel quantum technological schemes such as criticality-enhanced quantum sensing [70] and a squeezed vacuum state laser [71]. Notably, an exact solution for the AQRM with a biased term has been recently derived [72], and certain analytical solutions have been found via transcendental function extension [72,73] and transformation techniques [74,75]. Experimental realizations of the AQRM have been achieved in two-dimensional quantum wells [76], cavity quantum electrodynamics [77], and superconducting circuits [72]. The flexibility to adjust the RW and CRW coupling strengths renders the AQRM highly versatile. Indeed, this grants the ability to explore a plethora of coupling regimes, thereby enabling the creation of highly correlated nonclassical states. A pivotal question arises: Can we generate long-lived highly correlated nonclassical states that persist even in the presence of a reservoir at finite temperature? This question is of paramount importance for current experimental platforms.

In this paper, we demonstrate that long-lived highly correlated nonclassical states of the AQRM can indeed persist even in the presence of a reservoir at finite temperature. To support our theoretical findings, we use a quantum Markovian master equation to describe the evolution of the AQRM. This approach remains applicable across all coupling regimes, including degenerate points in the energy spectrum, i.e., without resorting to secular approximation. Consequently, such a quantum open system genuinely approaches a thermal Gibbs state as its steady state. Furthermore, through a series of complementary analyses, we characterize the *quantumness* of the steady state in the finite-temperature–coupling-strength phase diagram, showing that highly correlated nonclassical states can be achieved across a wide parameter region.

The rest of the paper is structured as follows: In Sec. II we present the open-system description of our model. In

Sec. III we briefly define the measures and witnesses of nonclassicality used throughout this paper. In Sec. IV, we outline our results, including the effects of temperature in the system. Finally, we present our concluding remarks in Sec. VI.

II. THE MODEL AND METHODS

The Hamiltonian of the AQRM [72] is ($\hbar = 1$)

$$\hat{H} = \omega \hat{a}^\dagger \hat{a} + \frac{\Delta}{2} \hat{\sigma}_z + \lambda_1 (\hat{a} \hat{\sigma}^+ + \hat{a}^\dagger \hat{\sigma}^-) + \lambda_2 (\hat{a}^\dagger \hat{\sigma}^+ + \hat{a} \hat{\sigma}^-). \quad (1)$$

This quantum system couples a two-level system (qubit) with a single-mode bosonic field undergoing both the RW and the CRW interaction terms unevenly. Here, the qubit is described by Pauli matrices $\hat{\sigma}_{x,y,z}$, $\hat{\sigma}^\pm = (\hat{\sigma}_x \pm i\hat{\sigma}_y)/2$ and transition frequency Δ , whereas the boson field is described with frequency ω and annihilation (creation) operator \hat{a} (\hat{a}^\dagger). Finally, λ_1 (λ_2) accounts for the light-matter coupling strength for the RW (CRW) interaction, where $\lambda_2 = 0$ is the JCM limit, $\lambda_1 = 0$ is the anti-Jaynes-Cummings model (AJCM), and $\lambda_1 = \lambda_2$ is the isotropic QRM.

One key aspect of the AQRM in Eq. (1) is that it preserves the parity symmetry \mathbb{Z}_2 as in the isotropic model [38]. This fact can be evidenced by considering the total-number-of-excitations operator $\hat{n} = \hat{a}^\dagger \hat{a} + \hat{\sigma}^+ \hat{\sigma}^-$ and the parity operator $\hat{\pi} = \exp(i\pi \hat{n})$. One can readily notice that, as opposed to the JCM, for the AQRM case $[\hat{H}, \hat{n}] \neq 0$ and $[\hat{H}, \hat{\pi}] = 0$. The above has two immediate consequences: (i) Even in the ground state, the expected mean number of qubit and boson excitations is nonzero, and (ii) it implies that $\hat{\pi}$ possesses two eigenvalues, $\langle \hat{\pi} \rangle = \pm 1$, depending on whether the total number of excitations is even or odd. This in turn enables us to solve the AQRM analytically using similar techniques to those used for the isotropic case, for instance, the Bargmann-Fock space of analytic functions and the Bogoliubov operator approach.

To gain a clearer understanding of the energy levels of the AQRM, in Fig. 1, we plot the energy spectrum in relation to the ground-state energy as a function of the light-matter coupling λ_1 (λ_2) for several coupling ratios λ_2/λ_1 (λ_1/λ_2). As seen from the figure, the spectrum exhibits level crossings where the ground-state parity changes sign (see green circles), leading the system to undergo infinite first-order quantum phase transitions as the coupling strength increases. In addition to the above degenerate crossing, several other nondegenerate and quasidegenerate points can be observed. The analysis of the AQRM spectrum, as shown in Fig. 1, is important for understanding the physics underlying the emergence of thermal correlations, a study that we will address in later sections.

As stated before, the central objective of this paper is to study the quantum correlations and quantum nonclassicality which remain present even at thermal equilibrium—the so-called thermal correlations and thermal nonclassicality of the AQRM, respectively. To see quantum thermalization and thermal entanglement in the open JCM [78] and QRM [79] as particular cases of the AQRM, we obtain the AQRM steady state when such a system interacts unavoidably with

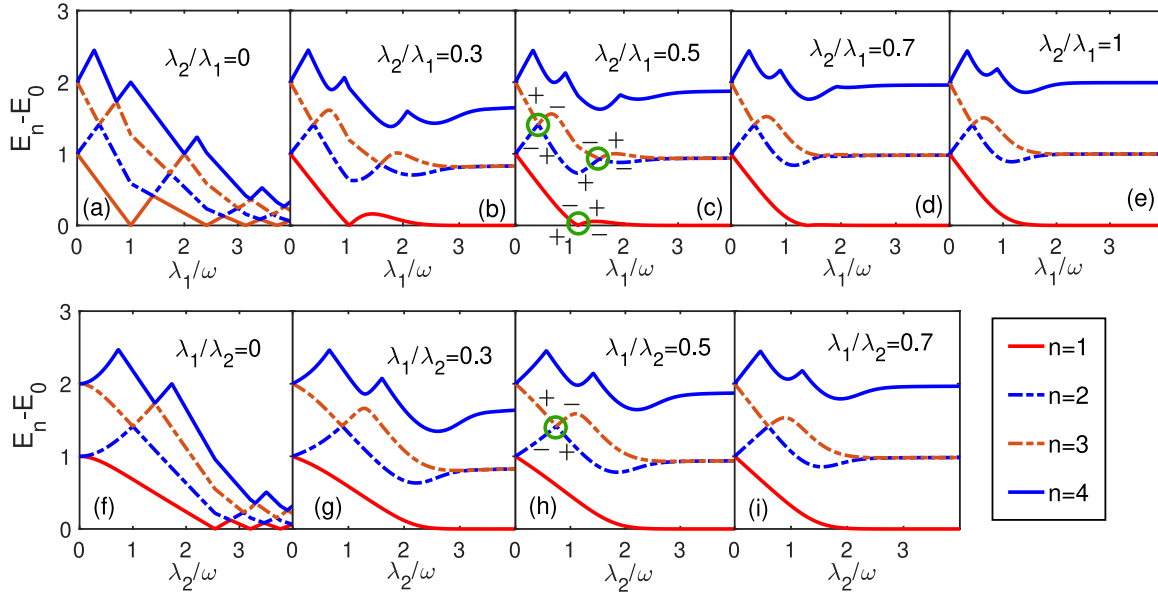


FIG. 1. Energy level differences are plotted as functions of the light-matter coupling strengths λ_1 (λ_2) for different coupling ratios λ_2/λ_1 (λ_1/λ_2). In (c) and (h), the green circles represent the (degenerate) crossing of the energy levels, and the plus and minus signs denote the change of parity of the energy levels. Other system parameters are specified as $\Delta = 1$ and $\omega = 1$.

a reservoir at temperature T . It is essential to point out that even though the standard Born-Markov master equation accurately describes the quantum state within the weak coupling regime $\lambda_i \ll \{\omega, \Delta\}$, it breaks down for stronger coupling regimes such as the USC and DSC regimes [37,38,80]. Consequently, the steady state at thermal equilibrium cannot be fully captured using the standard master equation in those regimes. To ensure that the steady state is the actual quantum state at thermal equilibrium for an arbitrary set of coupling strengths λ_i , one needs to switch to a Born-Markov master equation in a dressed picture [81]; see Refs. [82,83] for a similar approach in the Jaynes-Cummings (JC) case. In this more suitable representation, the quantum jumps occur between the dressed eigenstates of the full Hamiltonian, as opposed to the standard master equation, where the upward and downward jumps only consider the free energy of the Hamiltonian.

We emphasize that the AQRM spectrum (see Fig. 1) shows nondegenerate and degenerate eigenvalues which are appropriately modeled by the secular approximation in the derivation of the Markovian master equation, but it fails in the quasidegenerate case. Following the steps of Ref. [84], we can derive a valid master equation for the entire spectrum of the Hamiltonian equation (1); as long as we consider weak damping, a high bath cutoff frequency, and a flat spectral density, these are sufficient conditions to ensure positivity and Markovianity. Indeed, the dissipative dynamics undergoes the following dressed master equation:

$$\begin{aligned} \frac{d}{dt} \hat{\rho} = & -i[\hat{H}, \hat{\rho}] + \sum_{\substack{u=a,\sigma^- \\ k < j}} \{ \Gamma_u^{jk} n_u(\Delta_{jk}) \mathfrak{D}[\phi_j] \langle \phi_k |, \hat{\rho} \} \\ & + \Gamma_u^{jk} [1 + n_u(\Delta_{jk})] \mathfrak{D}[\phi_k] \langle \phi_j |, \hat{\rho} \} = \mathcal{L}(t) \rho, \end{aligned} \quad (2)$$

with the Liouvillian superoperator $\mathcal{L}(t)$ and Lindbladian terms defined as

$$\mathfrak{D}[\hat{O}, \hat{\rho}] = \frac{1}{2} [2\hat{O}\hat{\rho}\hat{O}^\dagger - \hat{\rho}\hat{O}^\dagger\hat{O} - \hat{O}^\dagger\hat{O}\hat{\rho}]. \quad (3)$$

In Eq. (2), $|\phi_k\rangle$ is the eigenvector of the AQRM, namely

$$\hat{H}|\phi_k\rangle = E_k|\phi_k\rangle, \quad (4)$$

where E_k is the k th eigenenergy associated with the eigenstate $|\phi_k\rangle$. We also define the dissipation rates

$$\Gamma_u^{jk} = \gamma_u(\Delta_{jk}) |S_u^{jk}|^2, \quad (5)$$

with two explicit contributions.

(i) The first contribution is the spectral function

$$\gamma_u(\Delta_{jk}) = 2\pi \sum_k |\lambda_{k,u}|^2 \delta(\Delta_{jk} - \omega_k), \quad (6)$$

where $\lambda_{k,u}$ accounts for the u th thermal bath coupled to a single-mode boson field with the frequency ω_k and energy gap

$$\Delta_{jk} = E_j - E_k. \quad (7)$$

(ii) The second contribution consists of the transition coefficients

$$S_q^{jk} = \langle \phi_j | (\hat{\sigma}_+ + \hat{\sigma}_-) | \phi_k \rangle, \quad (8)$$

$$S_c^{jk} = \langle \phi_j | (\hat{a}^\dagger + \hat{a}) | \phi_k \rangle. \quad (9)$$

To satisfy the necessary conditions for the validity of the above master equation, we consider the Ohmic case:

$$\gamma_u(\Delta_{jk}) = \pi \alpha \Delta_{jk} e^{-|\Delta_{jk}|/\omega_c}, \quad (10)$$

where α is the coupling strength between the system and the environment and ω_c is the cutoff frequency of thermal baths. Throughout all numerical simulations performed, we consider $\alpha = 0.001\omega$ and $\omega_c = 10\omega$. We note that for Gibbs states of the reservoir at temperature T , the correlation functions also obey the Kubo-Martin-Schwinger (KMS) relations [81], i.e., $\gamma_u(-\Delta_{jk}) = \gamma_u(\Delta_{jk}) e^{-\Delta_{jk}/k_B T}$, where k_B is the Boltzmann constant.

Finally, the temperature of the bath is encoded in the Bose-Einstein distribution ($k_B = 1$)

$$n_u(\Delta_{jk}, T_u) = \frac{1}{e^{\Delta_{jk}/T_u} - 1}. \quad (11)$$

It is important to emphasize that when both reservoirs have the same temperature $T_a = T_{\sigma^-}$ (or only one of the subsystems is coupled to the reservoir), the system reaches a thermal equilibrium. Consequently, the dressed master equation steady-state solution of Eq. (2) results in the density matrix of the canonical ensemble [a straightforward numerical simulation proves that the Gibbs state is indeed the steady-state solution of Eq. (2)]

$$\hat{\rho}_{\text{ss}} = \sum_k \frac{e^{-E_k/T}}{\mathcal{Z}} |\phi_k\rangle\langle\phi_k|, \quad (12)$$

where $\mathcal{Z} = \sum_k e^{-E_k/T}$ is the partition function and the steady-state population is

$$P_k = \frac{e^{-E_k/T}}{\mathcal{Z}}. \quad (13)$$

Notice that for unequal reservoir temperatures $T_a \neq T_{\sigma^-}$, the steady-state solution of the dressed master equation cannot be written in terms of the canonical ensemble as in Eq. (12). In what follows, we assume equal-temperature reservoirs such that we can always extract the statistical properties of the quantum state at thermal equilibrium from Eq. (12).

To shed light on the nature of the first-order phase transition in the AQRM shown in Fig. 1, we briefly investigate the Liouvillian \mathcal{L} spectrum [85]. This analysis not only determines the uniqueness of the equilibrium state described in Eq. (12), ruling out the possibility of a dissipative quantum phase transition, but also provides sufficient information to estimate the time scale required for relaxation. Let $\{\mu_\alpha\}_{\alpha=0,1,2,\dots}$ denote the complex eigenvalues of \mathcal{L} defined in Eq. (2) and presented in Figs. 2(a) and 2(b), for which we plot α up to ten eigenvalues for the representative temperatures of $T = 0.5\omega$ in Fig. 2(a) and $T = 0.1\omega$ in Fig. 2(b) for different coupling ratios λ_1/λ_2 and λ_2/λ_1 . In the current case of thermal AQRM, numerical evaluation indicates that $\mu_0 = 0$ is nondegenerate, thereby establishing a unique steady state as a consequence.

To assess the relaxation time scale, let us first examine the case of the decoupled system, where the cavity field mode at frequency ω interacts with a reservoir at temperature T . In this scenario, the average number of photons is given by $\langle \hat{a}^\dagger \hat{a} \rangle(t) = \langle \hat{a}^\dagger \hat{a} \rangle(0) e^{-\gamma(\omega)t} + n(\omega, T)(1 - e^{-\gamma(\omega)t})$. Thus one can define the thermalization time as $t_{th} = \gamma(\omega)^{-1}$. While the above time-scale analysis holds for the decoupled system, its thermalization time becomes highly nontrivial once nonzero coupling is taking into consideration. To explore the nontrivial effect of light-matter coupling on the thermalization time, we turn to the Liouvillian gap [86], which is defined as the difference between the zeroth (here $\mu_0 = 0$) and the first Liouvillian eigenvalues, i.e., $\mu_1 = -\max_{\alpha \neq 0} \text{Re}[\mu_\alpha]$. The Liouvillian gap determines the asymptotic decay rate and bounds the relaxation time in an equilibrium scenario as $t_{th} \approx |\mu_1|^{-1}$. To compare the relaxation time to achieve the equilibrium state of the AQRM, we plot in Figs. 2(c) and 2(d) the ratio between the Liouvillian gap $[\mu_1(\lambda_1)]$ normalized by the Liouvillian gap of the decoupled system $\mu_1(\lambda_1 = 0) = \gamma(\omega)$

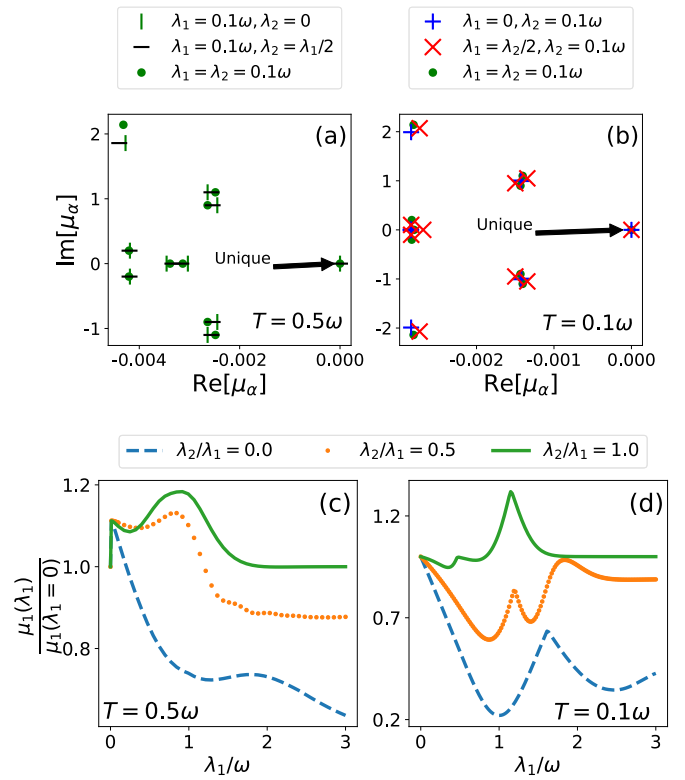


FIG. 2. (a) and (b) The imaginary and real parts of the first ten Liouvillian eigenvalues μ_α for different coupling ratios λ_1/λ_2 and λ_2/λ_1 and two different temperatures. For the representative parameters, the Liouvillian exhibits only one zero eigenvalue, indicating the uniqueness of the equilibrium state of the AQRM. (c) and (d) The ratio between the first eigenvalue of the Liouvillian (Liouvillian gap) normalized by the thermalization rate of the decoupled system $\mu_1(\lambda_1 = 0) = \gamma(\omega)$ as a function of λ_1 for several coupling ratios λ_2/λ_1 and two different temperatures.

for several coupling ratios λ_2/λ_1 and two different temperatures. As shown in the figure, the QRM (i.e., $\lambda_1 = \lambda_2$) requires a longer thermalization time over all coupling regimes λ_1/ω , and intriguingly, with the increasing coupling strength approaching the DSC regime, the relaxation time tends to be the same as that of the uncoupled system. Furthermore, the increase in anisotropy [e.g., $\lambda_2/\lambda_1 = 0.5$ in Figs. 2(c) and 2(d)] decreases the thermalization time, the JCM being the fastest to thermalize. Note that a faster thermalization time is crucial for some quantum processing tasks in quantum thermodynamics, where a shorter thermalization time, in principle, can increase the power of a quantum heat engine. The Liouvillian gap closure represents a distinctive feature of a dissipative quantum phase transition. In the case of the AQRM weakly coupled to a Markovian thermal reservoir, this closure is notably absent. This absence is clearly demonstrated in Figs. 2(c) and 2(d), where the gap remains nonzero for all temperatures and couplings considered.

III. QUANTUM CORRELATION AND NONCLASSICALITY MEASURES

The concept of quantumness (nonclassicality) is related to the impossibility of describing physical phenomena by

a deterministic or probabilistic classical theory. To understand the impact of the system's light-matter anisotropy on the thermal quantum correlations and thermal nonclassicality, i.e., quantum correlations and nonclassicality that are present at thermal equilibrium, we thoroughly study the following quantities: (i) the zero-delay second-order correlation function $g^{(2)}(0)$, (ii) the bosonic field quadrature squeezing ζ^2 , (iii) a phase-space interference macroscopicity measure $\mathcal{I}(\rho)$ for the quantum state ρ , (iv) the negativity $\mathcal{N}(\rho)$, and (v) the quantum discord $\mathcal{D}(\rho)$. In the subsequent sections, we briefly explain the above quantities.

A. Zero-delay second-order correlation function

While the Poissonian and the super-Poissonian photon statistics of a light beam can be entirely explained in terms of a classical theory of light, the occurrence of sub-Poissonian photon statistics characterizes the quantumness of photonic states without a classical counterpart. It is also relevant to point out that although this property does not consistently manifest in all quantum states of a field mode, a state can be classified as nonclassical when it is present. In this context, sub-Poissonian photon statistics serve as an authentic signature of the quantum nature of light.

Alternatively, one can classify the quantumness of a light beam by the study of the probabilities in measuring photons at a detector in a defined time interval $t_2 - t_1 \equiv \tau$, the so-called second-order correlation function $g^{(2)}(\tau)$. This definition classifies the light beam in a threefold fashion, namely: (i) $g^{(2)}(0) > 1$ [bunched light where photons populate themselves together (classically a chaotic description)], (ii) $g^{(2)}(0) = 1$ [random photon stream (classically a coherent description)], and (iii) $g^{(2)}(\tau) < 1$ [antibunched light where photons distribute separately (with no classical analogy)] [87,88], where we have considered an infinitesimal zero-delay time window $\tau \rightarrow 0$. Indeed, thermal photons emitted from noninteracting quantum modes or in the strong coupling regime are bunched ($g^{(2)}(0) = 2$), being the standard example of an incoherent source of light [87–89].

The conventional definition of the normalized zero-delay second-order correlation function is [90]

$$g^{(2)}(0) = \frac{\langle (\hat{a}^\dagger)^2 (\hat{a})^2 \rangle}{\langle \hat{a}^\dagger \hat{a} \rangle^2}. \quad (14)$$

This quantity describes the probability of detecting two photons simultaneously ($\tau \rightarrow 0$), which is normalized by the probability of detecting two photons at once within a random photon source. Nonetheless, this definition holds for weak light-matter couplings, where the intracavity photons, described by \hat{a} , suffice to explain the observed photon correlation. On the other hand, in the USC regime, where the qubit system strongly dresses the bosonic field, the second-order correlation function $g^{(2)}(0)$ is derived from the input-output formalism as [91,92]

$$G^{(2)}(0) = \frac{\langle (\hat{X}^-)^2 (\hat{X}^+)^2 \rangle}{\langle \hat{X}^- \hat{X}^+ \rangle^2}, \quad (15)$$

where

$$\hat{X}^+ = -i \sum_{k>j} \Delta_{kj} X_{jk} |\phi_j\rangle \langle \phi_k|, \quad (16)$$

with $\hat{X}^- = (\hat{X}^+)^\dagger$, $\Delta_{kj} = E_k - E_j$ being the energy gap, and $X_{jk} = \langle \phi_j | (\hat{a}^\dagger + \hat{a}) | \phi_k \rangle$. Here, X_{jk}^+ describes the transition from the higher eigenstate $|\phi_k\rangle$ to the lower one $|\phi_j\rangle$. Notice that in the weak light-matter interaction limit (i.e., $\lambda_i \ll 1$), the operator \hat{X}^+ is reduced to $\hat{X}^+ = -i\omega\hat{a}$. Thus the correlation function in Eq. (15) simplifies to the conventional case.

One fundamental observation regarding the second-order correlation function in Eq. (15) is that in the eigenbasis of the AQRM Hamiltonian shown in Eq. (1), the dressed light-matter jump operator \hat{X} provides an accurate expression for the average number of excitations in the ground state: $\langle \phi_0 | \hat{X}^- \hat{X}^+ | \phi_0 \rangle = 0$. This is in contrast to the seemingly incorrect result $\langle \phi_0 | \hat{a}^\dagger \hat{a} | \phi_0 \rangle \neq 0$. Note that as the dressed ground state can be spanned in the bare light-matter basis $\{|g\rangle, |e\rangle, |n\rangle\}$, the dressed ground state will be composed of a certain number of virtual excitations [93]. To convert the virtual excitations from the dressed picture into measurable photonic excitations, one can switch the interaction coupling strength on and off [93].

Indeed, consider a quantum state in the dressed basis $|\phi_k\rangle$. Once the interaction is switched off, the state will still contain the excitations that can now be detected using the intracavity photon operator \hat{a} . Hence $\langle \phi_k | \hat{a}^\dagger \hat{a} | \phi_k \rangle \neq 0$ will accurately describe the number of photonic excitations. It is worth noting that the nonadiabatic switch on or off needs to be of the order of the inverse of the relevant frequencies in the system, here ω, Δ [93].

The conversion between virtual excitations and real photons via switching the interaction on and off is a consistent way to reconcile the correlation functions and other quantities that describe the thermal quantum correlations and nonclassicality in this paper. Let us point out that the photons in the ground state of the USC models are virtual and cannot be detected [33], unless the coupling is suddenly switched off.

Throughout this paper, whenever a quantifier is defined using standard bosonic and spin operators, we refer to a scenario in which the coupling has been turned off after reaching thermal equilibrium.

B. Quadrature squeezing

The second-order correlation function fails as a nonclassical quantifier in the super-Poissonian regime. For instance, nonclassical Gaussian states, such as squeezed states, may show either photon bunching or photon antibunching depending on whether the amplitude fluctuations are increased or reduced. To reveal the nonclassicality present in the steady state of the AQRM field mode, we compute the degree of squeezing. To do so, we introduce the generalized rotated field quadrature $\sqrt{2}\hat{x}_\theta = \hat{a}e^{-i\theta} + \hat{a}^\dagger e^{i\theta}$, where any two operators that differ by $\theta = \pi/2$ form a conjugate pair which satisfies the position ($\theta = 0$) momentum ($\theta = \pi/2$) commutator relation. We consider the following squeezing parameter [94]:

$$\zeta^2 = \min_{\theta \in (0, 2\pi)} (\Delta \hat{x}_\theta)^2. \quad (17)$$

Only a value of $\zeta^2 < 1$ indicates bosonic squeezing, whereas $\zeta^2 = 1$ corresponds to the photonic coherent state of radiation field. The minimization in the above definition can be easily

obtained:

$$\zeta^2 = 1 + 2\langle \hat{a}^\dagger \hat{a} \rangle - 2|\langle \hat{a}^2 \rangle|, \quad (18)$$

where we have assumed that once the steady state is reached, the light-matter interaction is switched off. Note that Refs. [95,96] studied the squeezing of output quadratures in the USC-DSC regime through the dressed light-matter jump operators for a vacuum input field, which is the thermal equilibrium case considered here. Interestingly, the authors found that no open system in its ground state can produce output squeezing, even if its ground state is a squeezed state. Since most of the squeezing in the AQRM is present in the ground state, these generalized measures leads to zero degrees of squeezing in the thermal state if the coupling is on. For this reason, we only focus on evaluating the degree of squeezing once the light-matter interaction is switched off, i.e., ζ^2 .

C. Phase-space interference measure

To further study the nonclassicality of the AQRM steady state, we consider a phase-space interference measure that quantifies the degree of macroscopicity of the state [97], defined as

$$\mathcal{I} = -\frac{\pi}{2} \int dpdq W(q, p) \left(\frac{\partial^2}{\partial q^2} + \frac{\partial^2}{\partial p^2} + 1 \right), \quad (19)$$

where $W(q, p)$ is the Wigner function [53]. The macroscopicity \mathcal{I} takes a value of 0 for classical states, while for pure quantum states such as superpositions of coherent states, NOON states, and Fock states it corresponds to the average number of photons $\langle n \rangle$. In the case of the mixed state obtained by Eq. (12), the quantifier is constrained by the inequality $\mathcal{I}(\hat{\rho}_{ss}) < \text{Tr}(\hat{\rho}_{ss} \hat{a}^\dagger \hat{a})$.

D. Negativity

To explore the quantum correlations between the light-matter constituents, we commence by calculating the quantum entanglement within bipartite systems. Among the various entanglement quantifiers available, we opt to use the negativity $\mathcal{N}(\rho)$ [98–102]

$$\mathcal{N}(\rho) = \frac{\|\rho^{T_A}\|_1 - 1}{2}, \quad (20)$$

where ρ^{T_A} is the partial transpose of the quantum state ρ with respect to subsystem A and $\|Y\|_1 = \text{Tr}|Y| = \text{Tr}\sqrt{Y^\dagger Y}$ is the trace norm or the sum of the singular value the operator Y . Equivalently, the negativity can be computed as $\mathcal{N}(\rho) = 1/2 \sum_i (|\varepsilon_i| - \varepsilon_i)$, where ε_i are the eigenvalues of the partially transposed light-matter density matrix ρ . Note that $\mathcal{N}(\rho) = 0$ corresponds to separable (not entangled) quantum states.

E. Quantum discord

Quantum entanglement is not the sole manifestation of quantum correlations. In fact, quantum discord (QD) represents another measure of potential quantum correlations within a quantum system. This measure of correlation emerges from the observation that two classically equivalent methods of defining mutual information yield different outcomes within the quantum domain [103]. The QD of two

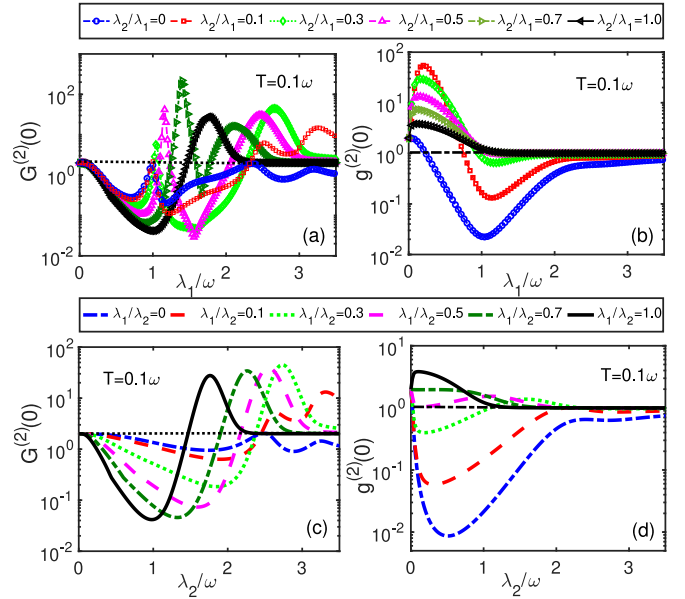


FIG. 3. Second-order correlation functions: (a) and (c) $G^{(2)}(0)$ as a function of the coupling strength λ_1 (λ_2) for several choices of coupling ratios λ_2/λ_1 (λ_1/λ_2). The black dotted horizontal line indicates $G^{(2)}(0) = 2$. (b) and (d) $g^{(2)}(0)$ as a function of λ_1 (λ_2) for different coupling ratios λ_2/λ_1 (λ_1/λ_2). The black dash-dotted horizontal line corresponds to $g^{(2)}(0) = 1$. The other system parameters are the same as in Fig. 1.

subsystems \mathcal{A} and \mathcal{B} can be expressed as [103]

$$\mathcal{D}(\hat{\rho}_{AB}) = S(\hat{\rho}_A) - S(\hat{\rho}_{AB}) + \min_{\{\Pi_j^A\}} S(\hat{\rho}_{B|\{\Pi_j^A\}}), \quad (21)$$

where $S(\hat{\rho}_i) = -\text{Tr}\hat{\rho}_i \log \hat{\rho}_i$ is the von Neumann entropy for the reduced density matrix and $S(\hat{\rho}_{B|\{\Pi_j^A\}})$ is the entropy conditioned through performing measurements on the \mathcal{A} system, defined as

$$S(\hat{\rho}_{B|\{\Pi_j^A\}}) = \sum_j p_j S(\{ \{\Pi_j^A\} \otimes I^B \} \hat{\rho}_{AB} \{ \{\Pi_j^A\} \otimes I^B \} / p_j). \quad (22)$$

In the above, Π_j^A is a von Neumann projection operator on subsystems \mathcal{A} , and $p_j = \text{Tr}(\{ \Pi_j^A \} \otimes I^B \hat{\rho}_{AB})$ is the probability with measurement outcome j . Note that one of the most distinct differences between QD and entanglement is that QD can be nonzero for certain separable states [9,104,105].

IV. QUANTUMNESS AT THERMAL EQUILIBRIUM

We commence by examining the impact of the light-matter coupling strengths, λ_1 and λ_2 , on the generation of long-lived quantum correlations in the AQRM. In Figs. 3(a) and 3(c), we plot the second-order correlation function using the dressed jump operator $G^{(2)}(0)$ as a function of the light-matter coupling strength λ_i ($i = 1, 2$) for several coupling ratios λ_i/λ_j ($i \neq j$) and a given temperature $T = 0.1\omega$. As Figs. 3(a) and 3(c) show, $G^{(2)}(0)$ generally transitions from photon antibunching [$G^{(2)}(0) < 1$] to photon bunching [$G^{(2)}(0) > 1$] as the light-matter coupling strength increases. In the limit of the DSC regime, i.e., $\lambda \gg \{\omega, \Delta\}$, the correlation function takes the value $G^{(2)}(0) = 2$, which corresponds to thermal photon

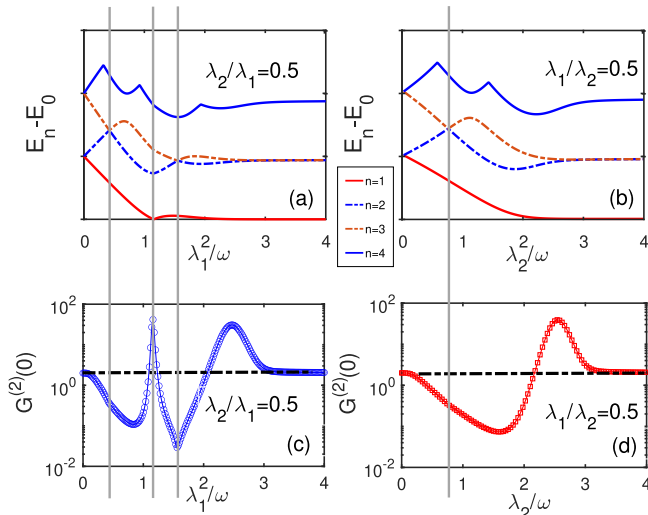


FIG. 4. Relationship between energy level crossing and the behavior of the second-order correlation function $G^{(2)}(0)$. (a) and (b) The energy gap $E_n - E_0$ of the AQRM as a function of λ_1 (λ_2) for $\lambda_2/\lambda_1 = 0.5$ ($\lambda_1/\lambda_2 = 0.5$); see more cases of coupling ratios in Fig. 1. (c) and (d) The particular case of $G^{(2)}(0)$ as a function of λ_1 (λ_2) for $\lambda_2/\lambda_1 = 0.5$ ($\lambda_1/\lambda_2 = 0.5$). The vertical gray lines evidence the correspondence between sharp peaks of $G^{(2)}(0)$ and the closing of energy gaps. Other system parameters are chosen as in Fig. 1.

emission (regardless of the coupling ratios). In Figs. 3(b) and 3(d), we depict the second-order correlation function using the bare jump operator $g^{(2)}(0)$ as a function of λ_i ($i = 1, 2$) for several coupling ratios λ_i/λ_j ($i \neq j$) and the same temperature $T = 0.1\omega$. As Figs. 3(b) and 3(d) show, the second-order correlation function $g^{(2)}(0)$ exhibits nonclassical features only for a strong degree of anisotropy (when the coupling strength ratio is small), i.e., $\lambda_2/\lambda_1 \leq 0.3$ and $\lambda_1/\lambda_2 \leq 0.3$, respectively. Interestingly, as the coupling ratios λ_i/λ_j increase, the nonclassical features (photonic antibunching effect) are completely suppressed [$g^{(2)}(0) > 1$]. Furthermore, with an increase in the light-matter coupling, $g^{(2)}(0)$ approaches unity regardless of the choice of coupling ratios. In other words, the thermal emission now displays the same statistical behavior as a coherent state. Note that in computing $g^{(2)}(0)$ using the bare bosonic field, we make the assumption that the coupling strength has been switched off [93] once the system has reached its thermal equilibrium. Notably, there is a significant distinction between the scenario in which the correlation function is computed from $G^{(2)}(0)$ and the one obtained when the light-matter coupling is switched off, resulting in $g^{(2)}(0)$. This subtlety demonstrates the intricate impact of virtual photonic excitations on the thermal state properties of the AQRM.

We can gain a clearer understanding of the second-order correlation function $G^{(2)}(0)$ by considering the energy level crossing and its associated change in parity, as similarly discussed in Ref. [106].

Consider the particular case of $G^{(2)}(0)$ as a function of λ_1 for a fixed coupling ratio $\lambda_2/\lambda_1 = 0.5$, as redrawn in Fig. 4(c) for clarity. The nonanalytical (sharp) peaks result from the energy level crossing depicted in Fig. 4(a) (see Fig. 1 for other choices of parameters). Indeed, the closing of the energy gap between higher excited states, namely the parity

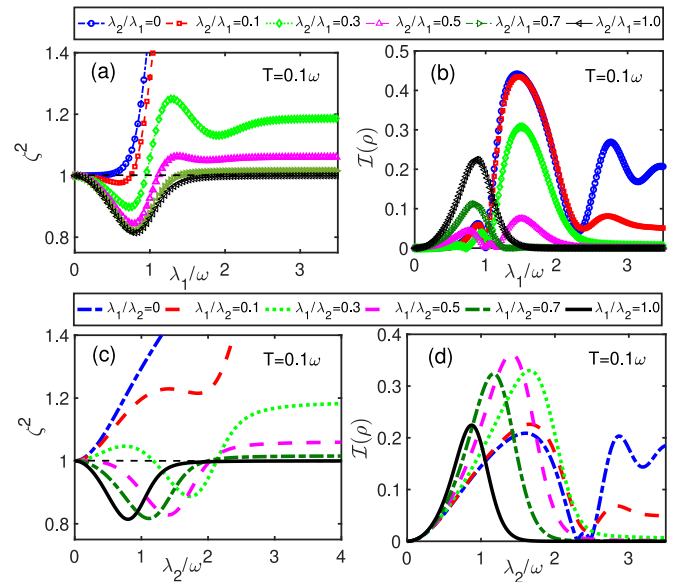


FIG. 5. (a) [(c)] The squeezing parameter ζ^2 as a function of λ_1 (λ_2) for different coupling ratios λ_2/λ_1 (λ_1/λ_2). The black dashed horizontal line corresponds to $\zeta^2 = 1$. (b) [(d)] The macroscopicity interference-based measure $\mathcal{I}(\rho)$ as a function of λ_1 (λ_2) for several coupling ratios λ_2/λ_1 (λ_1/λ_2). We consider a given temperature $T = 0.1\omega$, and other system parameters are the same as in Fig. 1.

change between the second (E_2) and the third (E_3) energy levels, is responsible for the antibunching peaks shown in Fig. 4(c). Furthermore, the closing of the energy gap between the ground state (E_0) and its first energy level (E_1) gives rise to the pronounced photonic bunched peak in Fig. 4(c) (around the value of $\lambda_1 \sim \omega$). Remarkably, the closing of the energy gap between E_1 and its ground state E_0 reopens as the coupling strength increases. This cycle of opening, closing, and reopening dynamics is responsible for the antibunched-bunched-antibunched behavior transition of $G^{(2)}(0)$ shown in Fig. 4(c). A similar analysis can be conducted for Fig. 4(d), in which we present $G^{(2)}(0)$ as a function of λ_2 for a fixed coupling ratio $\lambda_1/\lambda_2 = 0.5$. In contrast to the previous scenario, no nonanalytic behavior is observed. This is because although a crossing of energy levels between the second and third eigenenergies occurs, the energy gap between the ground state and the first excited state monotonically vanishes as the coupling strength increases. As a result, a smooth transition towards a photonic bunching effect takes place.

To investigate the degree of photonic squeezing, in Fig. 5(a) [Fig. 5(c)] we plot the squeezing parameter ζ^2 as a function of λ_1 (λ_2) for several coupling ratios λ_2/λ_1 (λ_1/λ_2) for a given temperature $T = 0.1\omega$. As the figures show, there is a clear degree of squeezing, $\zeta^2 < 1$, of the AQRM steady state (after the interaction has been switched off) for certain coupling ratios and a specific window of light-matter coupling. Note that for the JCM ($\lambda_2/\lambda_1 = 0$), no squeezing is achieved, i.e., $\zeta^2 \geq 1$, for all values of λ_1 . Conversely, for the QRM ($\lambda_2 = \lambda_1$), the degree of squeezing tends to a photonic coherent field as the light-matter coupling strength goes towards the USC-DSC regime. Notably, no photonic squeezing occurs for the high-anisotropy regime ($\lambda_i/\lambda_j \ll 1$, $i \neq j$). For

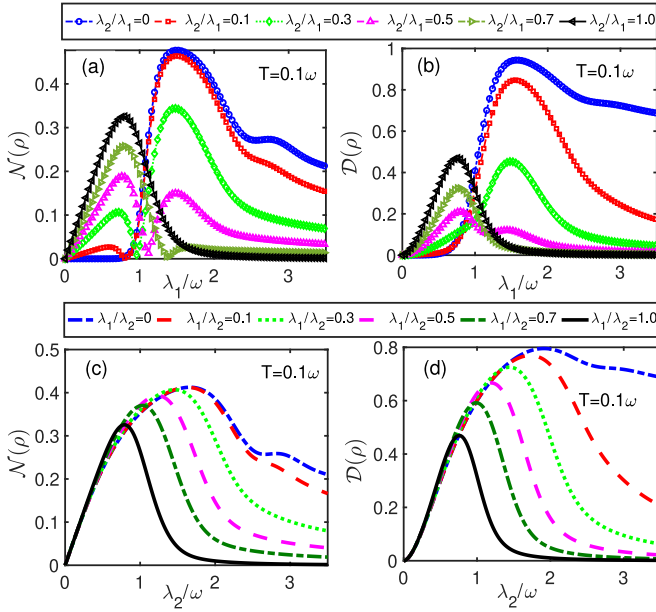


FIG. 6. (a) [(c)] The steady-state negativity $\mathcal{N}(\rho)$ as a function of λ_1 (λ_2) for different coupling ratios λ_2/λ_1 (λ_1/λ_2). (b) [(d)] The steady-state quantum discord $\mathcal{D}(\rho)$ as a function of λ_1 (λ_2) for several coupling ratios λ_2/λ_1 (λ_1/λ_2). We consider a given temperature $T = 0.1\omega$, and the other system parameters are the same as in Fig. 1.

instance, consider $\lambda_2/\lambda_1 = 0.1$ and $\lambda_1/\lambda_2 = 0.1$ in Figs. 5(a) and 5(c), respectively. As seen from the figures, no relevant photonic squeezing is achieved with the increasing of the light-matter coupling. This nonclassicality measure is in stark contrast with the second-order correlation function $g^{(2)}(0)$ (we recall that both cases are evaluated by turning the coupling off), for which it presents a high degree of nonclassicality in the region of high anisotropy.

To further evidence quantum features of the steady-state AQRM field that may have not been captured by previous quantifiers, in Fig. 5(b) [Fig. 5(d)] we show the macroscopicity interference-based measure $\mathcal{I}(\rho)$ as a function of λ_1 (λ_2) for different coupling ratios λ_2/λ_1 (λ_1/λ_2) and $T = 0.1\omega$. As the figures show, the higher degree of the interference-based measure generally occurs in the coupling region $1 < \lambda_i/\omega < 2$ ($i = 1, 2$) for most of the coupling ratios of anisotropies, where quantum squeezing did not capture such a nonclassical behavior but it appears to be closer to capturing the second-order correlation quantifier. Interestingly, as shown in Fig. 5(b), $\mathcal{I}(\rho)$ increases with increasing anisotropy, thus exhibiting clear quantum signatures in the DSC regime. In contrast, in Fig. 5(d), $\mathcal{I}(\rho)$ is maximum for $\lambda_1/\lambda_2 = 0.5$, which is a maximum of nonclassicality that is hidden in the previous measures.

Now, we study the thermal quantum correlations between the photons and the qubit through the quantifiers of negativity $\mathcal{N}(\rho)$ and quantum discord $\mathcal{D}(\rho)$. In Fig. 6(a), we plot the steady-state negativity $\mathcal{N}(\rho)$ as a function of λ_1 for several coupling ratios λ_2/λ_1 for $T = 0.1\omega$. As the figure shows, at some coupling ratios such as $\lambda_2/\lambda_1 = 0.1, 0.3, 0.5, 0.7$, the negativity shows a clear dip, nearly to zero, between two maxima. This minimum of near zero corresponds to the en-

ergy level crossing of the ground state and the first excited state; see Figs. 1(b)–1(d). In the case of the JCM ($\lambda_2/\lambda_1 = 0$), the steady-state negativity $\mathcal{N}(\rho)$ is nearly zero for coupling strengths $\lambda_1 \leq 0.7\omega$. However, as the coupling strength λ_1 increases, the negativity gradually rises until it reaches the highest degree of entanglement compared with any other coupling rate. In the case of the QRM ($\lambda_2/\lambda_1 = 1$), $\mathcal{N}(\rho)$ exhibits a single maximum with the highest degree of entanglement for coupling strength $\lambda_1 < \omega$. In Fig. 6(c), we depict the steady-state negativity $\mathcal{N}(\rho)$ as a function of λ_2 for different coupling ratios λ_1/λ_2 at a fixed temperature of $T = 0.1\omega$. As observed in the figure, the $\mathcal{N}(\rho)$ exhibits a smooth behavior without a sudden drop to near zero. This is because, in contrast to the previous scenario, there is no energy level crossing between the ground state and the first excited state, as shown in Figs. 1(g)–1(i). While the steady-state negativity of Fig. 6(c) is qualitatively similar to the steady-state quantum discord $\mathcal{D}(\rho)$ of Fig. 6(d), the situation differs for Figs. 6(a) and 6(b). Indeed, in Fig. 6(b), we plot the quantum discord $\mathcal{D}(\rho)$ as a function of λ_1 for several coupling ratios λ_2/λ_1 for $T = 0.1\omega$. As the figure shows, its overall profile is similar to that of Fig. 6(a); this means that almost all nonlocal quantum correlations are due to entanglement. However, unlike the negativity shown in Fig. 6(a), at the crossing of the ground state and the first excited state the quantum discord $\mathcal{D}(\rho)$ does not decrease to near zero for some coupling strengths (e.g., $\lambda_2/\lambda_1 = 0.1, 0.3, 0.5, 0.7$). Thus we can infer the following: (i) All nonlocal quantum correlations are in the form of entanglement, (ii) the quantum correlations increase with anisotropy, and (iii) for high anisotropy they increase with the coupling strength presenting its maximum in the DSC regime.

It is worth noting that the system's behavior for increasing light-matter coupling, e.g., $\lambda_i \gtrsim 3\omega$ ($i = 1, 2$), qualitatively resembles the system's behavior for the decoupled light-matter case, i.e., $\lambda_i = 0$. Such a qualitative correspondence implies a trivial behavior of the quantifiers for very large light-matter interaction strengths, $\lambda_i \gtrsim 3\omega$ ($i = 1, 2$), and for anisotropies with values exceeding $\lambda_i/\lambda_j \geq 0.3$, where $i \neq j$; see Fig. 1. This behavior can be understood as, in the depths of the DSC regime, the spectrum becomes harmonic again (see Fig. 1 for $\lambda_i > 3\omega$), with the dressed states forming product states between displaced Fock photonic states and atomic states that are x polarized, leading to $G^{(2)}(0) = 2$. The nearly equal energy gaps (quasi-harmonic spectrum) and the eigenstates being product states in the DSC regime suggest that (i) there is no degree of squeezing and macroscopicity and (ii) the vanishing of quantum entanglement and quantum discord at all temperatures should be expected (as shown in Figs. 3–6).

V. ROBUSTNESS OF THERMAL QUANTUMNESS AT HIGHER TEMPERATURES

As temperatures rise, thermal fluctuations increase, thereby modifying the AQRM steady state as described in Eq. (12). On one hand, higher temperatures result in an increased expansion of states in the polariton basis, which may potentially lead to more frequent energy level crossings among higher AQRM eigenstates. On the other hand, these thermal fluctua-

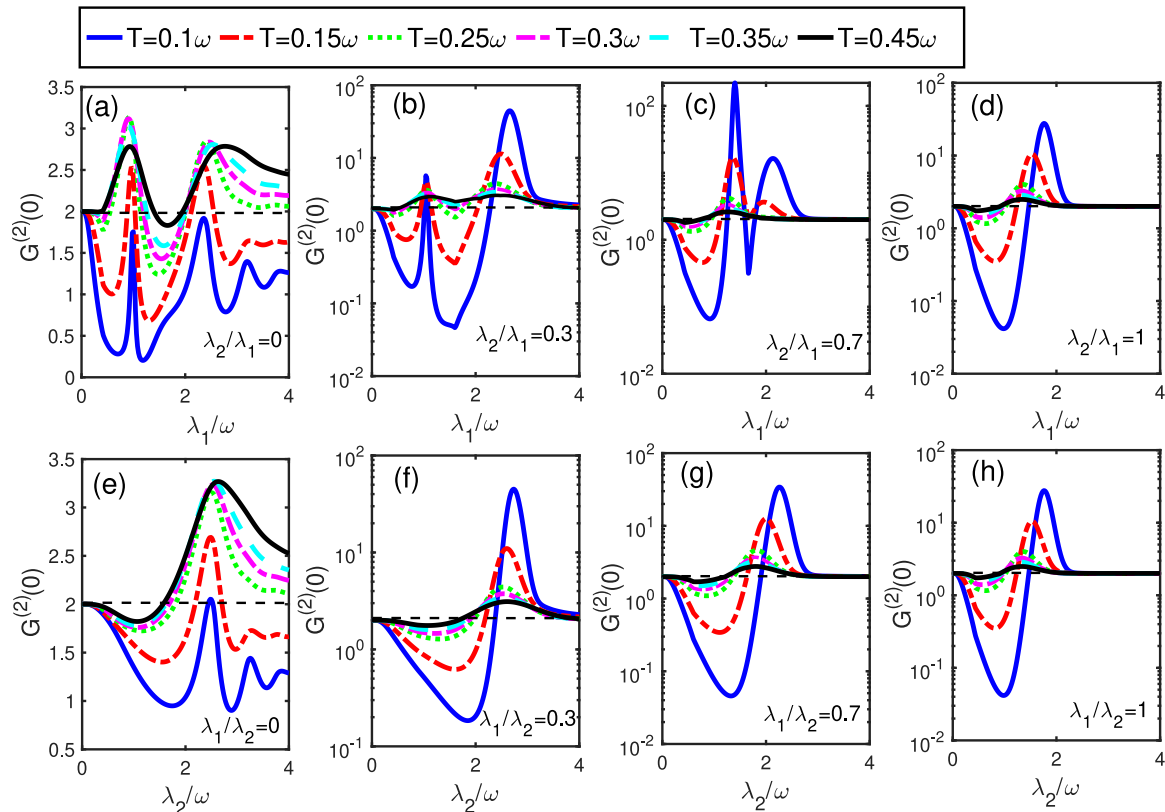


FIG. 7. (a)–(h) Second-order correlation function $G^{(2)}(0)$ as a function of the light-matter coupling λ_i ($i = 1, 2$) for several choices of coupling ratios λ_i/λ_j ($i \neq j$) and different temperatures T . The black dashed horizontal line corresponds to $G^{(2)}(0) = 2$. Other system parameters are as in Fig. 1.

tions may cause the system to lose its coherence, potentially having a detrimental impact on the AQRM steady state. To explore this nontrivial scenario, which involves a trade-off between increased energy level interplay and the influence of thermal fluctuations, we investigate how higher finite thermal bath temperatures affect the generation of nonclassical and quantum correlations in the AQRM, while considering all the above quantifiers.

In Fig. 7, we illustrate the second-order correlation function $G^{(2)}(0)$ as a function of the light-matter coupling λ_i ($i = 1, 2$) for several choices of coupling ratios λ_i/λ_j ($i \neq j$) and different temperatures T . As evident from the figure, the higher the anisotropy, the more robust the quantum correlations are in the presence of temperature fluctuations. Moreover, it exhibits a larger quantum region as a function of the coupling strengths. Notably, the correlation function $G^{(2)}(0)$ is prone to thermal decoherence, as signatures of nonclassicality (antibunching) survive only at temperatures as high as $T \sim 0.15\omega$, as depicted in all panels of Fig. 7. For higher temperatures, the antibunching effect is largely suppressed with increasing temperature for the same values of the coupling ratio, suggesting that thermodynamic fluctuations consistently destroy nonclassical features in high-temperature regions.

In Fig. 8, we show the temperature effects on the four quantifiers, namely ζ^2 , $\mathcal{I}(\rho)$, $\mathcal{N}(\rho)$, and $\mathcal{D}(\rho)$, as functions of the light-matter coupling λ_i ($i = 1, 2$) and the temperature T for different coupling ratios λ_i/λ_j ($i \neq j$).

In the first row of Fig. 8, we plot the squeezing parameter ζ^2 as functions of λ_i ($i = 1, 2$) and T for different λ_i/λ_j ($i \neq j$) values. Specifically, as observed in Figs. 8(a) and 8(d), no squeezing effect is achieved in the specific cases of the JCM ($\lambda_2 = 0$) and the AJCM ($\lambda_1 = 0$). However, for other coupling ratios, significant squeezing effects are observed at temperatures around $T \approx 0.3\omega$. Such a high degree of squeezing is attained by decreasing the anisotropy, making the Rabi model the ideal scenario for obtaining this resource.

In the second row of Fig. 8, we depict the macroscopicity interference-based measure $\mathcal{I}(\rho)$ as functions of λ_i ($i = 1, 2$) and T for different λ_i/λ_j ($i \neq j$) values. Unlike in the case of the squeezing parameter, the macroscopicity interference-based measure for the JCM and AJCM cases is nonzero, as shown in Figs. 8(h) and 8(k). It is worth noting that the macroscopicity takes nonzero values over a broader range of coupling strengths compared with other ratios at low temperatures $T < 0.1\omega$. However, as the figure shows, this quantifier is more susceptible to thermal fluctuations originating from the thermal reservoir and practically disappears for temperatures $T > 0.1\omega$.

Lastly, in the third and fourth rows of Fig. 8, we depict steady-state quantum entanglement $\mathcal{N}(\rho)$ and quantum discord $\mathcal{D}(\rho)$. Both quantifiers exhibit qualitatively similar behaviors. Similar to the macroscopicity interference-based measure, both quantifiers are more pronounced over a broader range of coupling strengths and temperatures. As the ratio λ_2/λ_1 (λ_1/λ_2) increases, the range in which both quantifiers

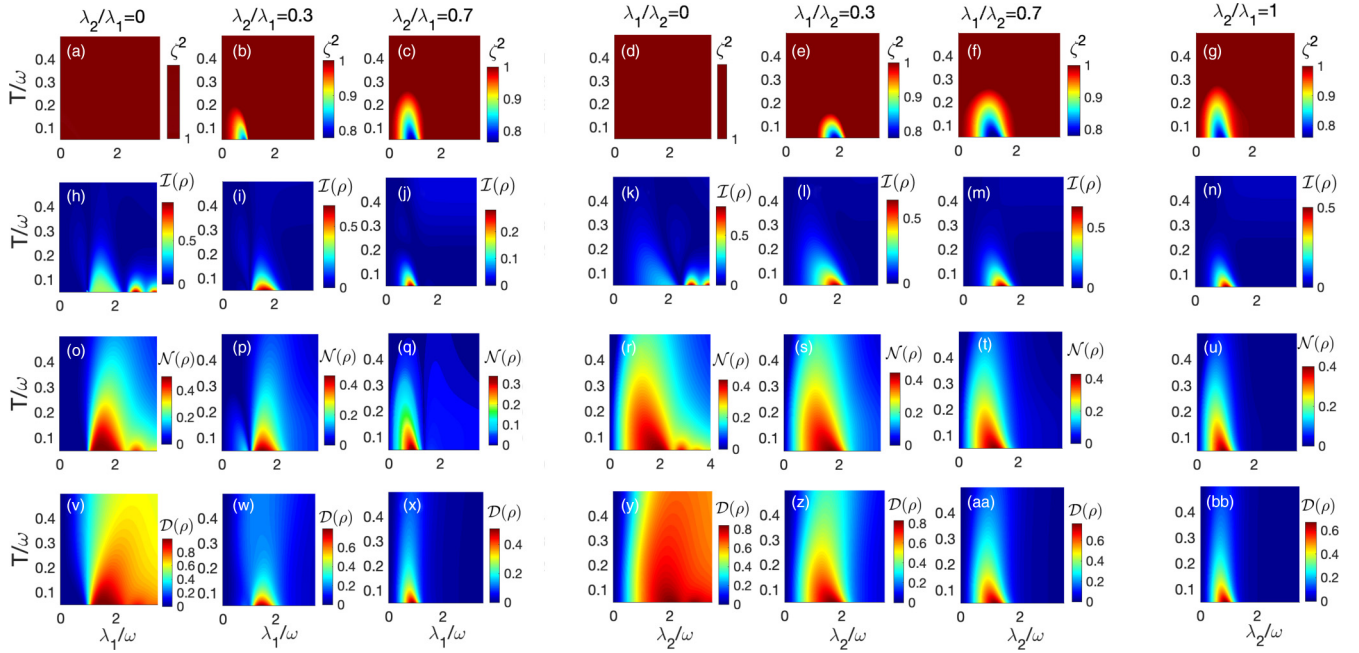


FIG. 8. The phase diagram of the (a)–(g) squeezing parameter ζ^2 , (h)–(n) macroscopicity $\mathcal{I}(\rho)$, (o)–(u) negativity $\mathcal{N}(\rho)$, and (v)–(bb) quantum discord $\mathcal{D}(\rho)$, as functions of the light-matter coupling λ_i ($i = 1, 2$) and the temperature T for different coupling ratios λ_i/λ_j ($i \neq j$). Other system parameters are as in Fig. 1.

appear gradually narrows. In the case of $0 < \lambda_2/\lambda_1 < 1$, as λ_1 changes, quantum entanglement $\mathcal{N}(\rho)$ appears in two regions, with a value of zero between these two regions. This result is due to the energy level crossing between the ground state and the first excited state. However, for quantum discord $\mathcal{D}(\rho)$, only one region appears. Interestingly, in the case of high anisotropy, entanglement persists up to temperatures $T \approx 0.3\omega$, while quantum discord demonstrates greater robustness in the presence of thermal fluctuations up to temperatures $T \lesssim 0.4\omega$.

Our theoretical proposal to reach nonclassical equilibrium states not only is of academic interest but also meets the present-day nontrivial experimental challenges, mainly involving the coupling strength and low-temperature environments. On the one hand, the physical model considered is general and has been implemented in a large number of systems, such as cavity quantum electrodynamics [77] and superconducting circuits [72]. Among them, the USC regime has been experimentally demonstrated for more than a decade [36] ($\lambda/\omega > 0.1$). Since then, the USC regime has been achieved in several other systems [38]. On the other hand, the DSC regime is within the reach of experimental techniques, notably in Ref. [39] in a circuit quantum electrodynamics setup implementing the QRM, for the highest reported strength of light-matter interaction of $\lambda/\omega \approx 1.34$ with temperature of approximately 45 mK ($k_B T/\hbar\omega \approx 0.16$), where thermal entanglement was also confirmed.

VI. CONCLUSION

In this paper, we consider the steady state of the AQRM by solving a dressed master equation at thermal equilibrium. Such a master equation in the dressed basis is valid for any light-matter coupling strength, and where the resulting steady

state is indeed a Gibbs state. Our findings are twofold: (i) We investigated the generation of quantum correlations and nonclassicality in the AQRM steady state at thermal equilibrium. Through a comprehensive analysis of various measures of quantum correlation and nonclassicality, we demonstrate that quantum effects persist across a broad range of anisotropies and coupling strengths, even at moderate thermal equilibrium temperatures. (ii) Such quantum features significantly emerge in the USC regime and at the onset of the DSC regime, while practically vanishing in the deeper DSC regime. In the dressed picture, this results in virtual field excitations within the system. Notably, we show a significant difference in the second-order correlation function when computed using dressed jump operators compared with using bare field operators (i.e., when the light-matter coupling is assumed to be switched off after the system reaches thermal equilibrium). Both the difference between these quantifiers and the persisting quantum features of the AQRM steady state at high temperatures could allow for experimental approaches to study the impact of virtual excitations in the USC regime. In particular, the quantum features emerging from the system avoid the need for demanding ground-state cooling.

ACKNOWLEDGMENTS

H.-G.X. and J.J. are supported by National Natural Science Foundation of China under Grant No. 11975064. V.M. thanks the National Natural Science Foundation of China (Grants No. 12050410251 and No. 12374482) and the Postdoctoral Science Foundation of China (Grant No. 2022T150098). G.X. acknowledges the support of NSF of China under Grant No. 12174346.

- [1] E. Chitambar and G. Gour, Quantum resource theories, *Rev. Mod. Phys.* **91**, 025001 (2019).
- [2] A. Streltsov, G. Adesso, and M. B. Plenio, Colloquium: Quantum coherence as a resource, *Rev. Mod. Phys.* **89**, 041003 (2017).
- [3] A. Acín, I. Bloch, H. Buhrman, T. Calarco, C. Eichler, J. Eisert, D. Esteve, N. Gisin, S. J. Glaser, F. Jelezko, S. Kuhr, M. Lewenstein, M. F. Riedel, P. O. Schmidt, R. Thew, A. Wallraff, I. Walmsley, and F. K. Wilhelm, The quantum technologies roadmap: a European community view, *New J. Phys.* **20**, 080201 (2018).
- [4] M. A. Nielsen and I. L. Chuang, *Quantum Computation and Quantum Information* (Cambridge University Press, Cambridge, 2010).
- [5] W. H. Zurek, Decoherence, einselection, and the quantum origins of the classical, *Rev. Mod. Phys.* **75**, 715 (2003).
- [6] S. Bose, A. Mazumdar, G. W. Morley, H. Ulbricht, M. Toroš, M. Paternostro, A. A. Geraci, P. F. Barker, M. S. Kim, and G. Milburn, Spin entanglement witness for quantum gravity, *Phys. Rev. Lett.* **119**, 240401 (2017).
- [7] C. Marletto and V. Vedral, Gravitationally induced entanglement between two massive particles is sufficient evidence of quantum effects in gravity, *Phys. Rev. Lett.* **119**, 240402 (2017).
- [8] K. Modi, A. Brodutch, H. Cable, T. Paterek, and V. Vedral, The classical-quantum boundary for correlations: Discord and related measures, *Rev. Mod. Phys.* **84**, 1655 (2012).
- [9] R. Coto, V. Montenegro, V. Ereemeev, D. Mundarain, and M. Orszag, The power of a control qubit in weak measurements, *Sci. Rep.* **7**, 6351 (2017).
- [10] L. Amico, R. Fazio, A. Osterloh, and V. Vedral, Entanglement in many-body systems, *Rev. Mod. Phys.* **80**, 517 (2008).
- [11] S. Boixo, S. V. Isakov, V. N. Smelyanskiy, R. Babbush, N. Ding, Z. Jiang, M. J. Bremner, J. M. Martinis, and H. Neven, Characterizing quantum supremacy in near-term devices, *Nat. Phys.* **14**, 595 (2018).
- [12] J. Preskill, Quantum computing in the NISQ era and beyond, *Quantum* **2**, 79 (2018).
- [13] N. Gisin and R. Thew, Quantum communication, *Nat. Photonics* **1**, 165 (2007).
- [14] V. Scarani, H. Bechmann-Pasquinucci, N. J. Cerf, M. Dušek, N. Lütkenhaus, and M. Peev, The security of practical quantum key distribution, *Rev. Mod. Phys.* **81**, 1301 (2009).
- [15] C. L. Degen, F. Reinhard, and P. Cappellaro, Quantum sensing, *Rev. Mod. Phys.* **89**, 035002 (2017).
- [16] V. Giovannetti, S. Lloyd, and L. Maccone, Advances in quantum metrology, *Nat. Photonics* **5**, 222 (2011).
- [17] V. Giovannetti, S. Lloyd, and L. Maccone, Quantum metrology, *Phys. Rev. Lett.* **96**, 010401 (2006).
- [18] V. Giovannetti, S. Lloyd, and L. Maccone, Quantum-enhanced measurements: Beating the standard quantum limit, *Science* **306**, 1330 (2004).
- [19] V. Montenegro, M. G. Genoni, A. Bayat, and M. G. A. Paris, Quantum metrology with boundary time crystals, *Commun. Phys.* **6**, 304 (2023).
- [20] V. Montenegro, M. G. Genoni, A. Bayat, and M. G. A. Paris, Probing of nonlinear hybrid optomechanical systems via partial accessibility, *Phys. Rev. Res.* **4**, 033036 (2022).
- [21] V. Montenegro, M. G. Genoni, A. Bayat, and M. G. A. Paris, Mechanical oscillator thermometry in the nonlinear optomechanical regime, *Phys. Rev. Res.* **2**, 043338 (2020).
- [22] I. M. Georgescu, S. Ashhab, and F. Nori, Quantum simulation, *Rev. Mod. Phys.* **86**, 153 (2014).
- [23] D. Suter and G. A. Álvarez, Colloquium: Protecting quantum information against environmental noise, *Rev. Mod. Phys.* **88**, 041001 (2016).
- [24] V. Ereemeev, V. Montenegro, and M. Orszag, Thermally generated long-lived quantum correlations for two atoms trapped in fiber-coupled cavities, *Phys. Rev. A* **85**, 032315 (2012).
- [25] L.-M. Duan and G.-C. Guo, Preserving coherence in quantum computation by pairing quantum bits, *Phys. Rev. Lett.* **79**, 1953 (1997).
- [26] D. Mundarain and M. Orszag, Decoherence-free subspace and entanglement by interaction with a common squeezed bath, *Phys. Rev. A* **75**, 040303(R) (2007).
- [27] D. A. Lidar, I. L. Chuang, and K. B. Whaley, Decoherence-free subspaces for quantum computation, *Phys. Rev. Lett.* **81**, 2594 (1998).
- [28] D. A. Lidar, D. Bacon, J. Kempe, and K. B. Whaley, Protecting quantum information encoded in decoherence-free states against exchange errors, *Phys. Rev. A* **61**, 052307 (2000).
- [29] L. Viola and E. Knill, Random decoupling schemes for quantum dynamical control and error suppression, *Phys. Rev. Lett.* **94**, 060502 (2005).
- [30] L. C. Celeri, M. A. de Ponte, C. J. Villas-Boas, and M. H. Y. Moussa, Switching off the reservoir through nonstationary quantum systems, *J. Phys. B: At. Mol. Opt. Phys.* **41**, 085504 (2008).
- [31] F. Reiter, D. Reeb, and A. S. Sørensen, Scalable dissipative preparation of many-body entanglement, *Phys. Rev. Lett.* **117**, 040501 (2016).
- [32] G. D. de Moraes Neto, V. F. Teizen, V. Montenegro, and E. Vernek, Steady many-body entanglements in dissipative systems, *Phys. Rev. A* **96**, 062313 (2017).
- [33] G. D. de Moraes Neto, W. Rosado, F. O. Prado, and M. H. Y. Moussa, Steady entanglement in bosonic dissipative networks, *Phys. Rev. A* **90**, 062322 (2014).
- [34] A. Blais, S. M. Girvin, and W. D. Oliver, Quantum information processing and quantum optics with circuit quantum electrodynamics, *Nat. Phys.* **16**, 247 (2020).
- [35] G. Wendin, Quantum information processing with superconducting circuits: a review, *Rep. Prog. Phys.* **80**, 106001 (2017).
- [36] A. A. Anappara, S. De Liberato, A. Tredicucci, C. Ciuti, G. Biasiol, L. Sorba, and F. Beltram, Signatures of the ultrastrong light-matter coupling regime, *Phys. Rev. B* **79**, 201303(R) (2009).
- [37] T. Niemczyk, F. Deppe, H. Huebl, E. P. Menzel, F. Hocke, M. J. Schwarz, J. J. Garcia-Ripoll, D. Zueco, T. Hümmer, E. Solano, A. Marx, and R. Gross, Circuit quantum electrodynamics in the ultrastrong-coupling regime, *Nat. Phys.* **6**, 772 (2010).
- [38] P. Forn-Díaz, L. Lamata, E. Rico, J. Kono, and E. Solano, Ultrastrong coupling regimes of light-matter interaction, *Rev. Mod. Phys.* **91**, 025005 (2019).
- [39] F. Yoshihara, T. Fuse, S. Ashhab, K. Kakuyanagi, S. Saito, and K. Semba, Superconducting qubit-oscillator circuit beyond the ultrastrong-coupling regime, *Nat. Phys.* **13**, 44 (2017).

- [40] F. Yoshihara, T. Fuse, Z. Ao, S. Ashhab, K. Kakuyanagi, S. Saito, T. Aoki, K. Koshino, and K. Semba, Inversion of qubit energy levels in qubit-oscillator circuits in the deep-strong-coupling regime, *Phys. Rev. Lett.* **120**, 183601 (2018).
- [41] D. Meschede, H. Walther, and G. Müller, One-atom maser, *Phys. Rev. Lett.* **54**, 551 (1985).
- [42] R. J. Thompson, G. Rempe, and H. J. Kimble, Observation of normal-mode splitting for an atom in an optical cavity, *Phys. Rev. Lett.* **68**, 1132 (1992).
- [43] C. Weisbuch, M. Nishioka, A. Ishikawa, and Y. Arakawa, Observation of the coupled exciton-photon mode splitting in a semiconductor quantum microcavity, *Phys. Rev. Lett.* **69**, 3314 (1992).
- [44] P. Lodahl, S. Mahmoodian, and S. Stobbe, Interfacing single photons and single quantum dots with photonic nanostructures, *Rev. Mod. Phys.* **87**, 347 (2015).
- [45] X. Gu, A. F. Kockum, A. Miranowicz, Y.-x. Liu, and F. Nori, Microwave photonics with superconducting quantum circuits, *Phys. Rep.* **718-719**, 1 (2017).
- [46] S. Ashhab and F. Nori, Qubit-oscillator systems in the ultrastrong-coupling regime and their potential for preparing nonclassical states, *Phys. Rev. A* **81**, 042311 (2010).
- [47] L.-T. Shen, Z.-B. Yang, M. Lu, R.-X. Chen, and H.-Z. Wu, Ground state of the asymmetric rabi model in the ultrastrong coupling regime, *Appl. Phys. B* **117**, 195 (2014).
- [48] A. Ridolfo, S. Savasta, and M. J. Hartmann, Nonclassical radiation from thermal cavities in the ultrastrong coupling regime, *Phys. Rev. Lett.* **110**, 163601 (2013).
- [49] L. Garziano, A. Ridolfo, S. De Liberato, and S. Savasta, Cavity QED in the ultrastrong coupling regime: photon bunching from the emission of individual dressed qubits, *ACS Photonics* **4**, 2345 (2017).
- [50] I. I. Rabi, On the process of space quantization, *Phys. Rev.* **49**, 324 (1936).
- [51] I. I. Rabi, Space quantization in a gyrating magnetic field, *Phys. Rev.* **51**, 652 (1937).
- [52] D. Braak, Q.-H. Chen, M. T. Batchelor, and E. Solano, Semiclassical and quantum Rabi models: in celebration of 80 years, *J. Phys. A: Math. Theor.* **49**, 300301 (2016).
- [53] M. O. Scully and M. S. Zubairy, *Quantum Optics* (Cambridge University Press, Cambridge, 1997).
- [54] Q.-H. Chen, Y. Yang, T. Liu, and K.-L. Wang, Entanglement dynamics of two independent Jaynes-Cummings atoms without the rotating-wave approximation, *Phys. Rev. A* **82**, 052306 (2010).
- [55] F. Altintas, A. Ü. C. Hardal, and Ö. E. Müstecaplıoğlu, Rabi model as a quantum coherent heat engine: From quantum biology to superconducting circuits, *Phys. Rev. A* **91**, 023816 (2015).
- [56] M.-J. Hwang, R. Puebla, and M. B. Plenio, Quantum phase transition and universal dynamics in the Rabi model, *Phys. Rev. Lett.* **115**, 180404 (2015).
- [57] M.-J. Hwang, M. S. Kim, and M.-S. Choi, Recurrent delocalization and quasiequilibration of photons in coupled systems in circuit quantum electrodynamics, *Phys. Rev. Lett.* **116**, 153601 (2016).
- [58] M. Liu, S. Chesi, Z.-J. Ying, X. Chen, H.-G. Luo, and H.-Q. Lin, Universal scaling and critical exponents of the anisotropic quantum Rabi model, *Phys. Rev. Lett.* **119**, 220601 (2017).
- [59] D. Braak, Integrability of the Rabi model, *Phys. Rev. Lett.* **107**, 100401 (2011).
- [60] Q.-H. Chen, C. Wang, S. He, T. Liu, and K.-L. Wang, Exact solvability of the quantum Rabi model using Bogoliubov operators, *Phys. Rev. A* **86**, 023822 (2012).
- [61] E. T. Jaynes and F. W. Cummings, Comparison of quantum and semiclassical radiation theories with application to the beam maser, *Proc. IEEE* **51**, 89 (1963).
- [62] S. De Liberato, C. Ciuti, and I. Carusotto, Quantum vacuum radiation spectra from a semiconductor microcavity with a time-modulated vacuum Rabi frequency, *Phys. Rev. Lett.* **98**, 103602 (2007).
- [63] B. Peropadre, P. Forn-Díaz, E. Solano, and J. J. García-Ripoll, Switchable ultrastrong coupling in circuit QED, *Phys. Rev. Lett.* **105**, 023601 (2010).
- [64] P. Nataf and C. Ciuti, Vacuum degeneracy of a circuit QED system in the ultrastrong coupling regime, *Phys. Rev. Lett.* **104**, 023601 (2010).
- [65] J. Casanova, G. Romero, I. Lizuain, J. J. García-Ripoll, and E. Solano, Deep strong coupling regime of the Jaynes-Cummings model, *Phys. Rev. Lett.* **105**, 263603 (2010).
- [66] W.-J. Yang and X.-B. Wang, Ultrastrong-coupling quantum-phase-transition phenomena in a few-qubit circuit QED system, *Phys. Rev. A* **95**, 043823 (2017).
- [67] L.-T. Shen, Z.-B. Yang, H.-Z. Wu, and S.-B. Zheng, Quantum phase transition and quench dynamics in the anisotropic Rabi model, *Phys. Rev. A* **95**, 013819 (2017).
- [68] C. Joshi, J. Larson, and T. P. Spiller, Quantum state engineering in hybrid open quantum systems, *Phys. Rev. A* **93**, 043818 (2016).
- [69] T. Ye, C. Wang, and Q.-H. Chen, Implication of giant photon bunching on quantum phase transition in the dissipative anisotropic quantum Rabi model, *Phys. A (Amsterdam)* **609**, 128364 (2023).
- [70] X. Zhu, J.-H. Lü, W. Ning, F. Wu, L.-T. Shen, Z.-B. Yang, and S.-B. Zheng, Criticality-enhanced quantum sensing in the anisotropic quantum Rabi model, *Sci. China Phys., Mech. Astron.* **66**, 250313 (2023).
- [71] F. de Oliveira Neto, G. D. de Moraes Neto, and M. H. Y. Moussa, A squeezed vacuum state laser with zero diffusion from cavity losses, *Ann. Phys. (Berlin)* **534**, 2100072 (2022).
- [72] Q.-T. Xie, S. Cui, J.-P. Cao, L. Amico, and H. Fan, Anisotropic Rabi model, *Phys. Rev. X* **4**, 021046 (2014).
- [73] X.-Y. Chen, L. Duan, D. Braak, and Q.-H. Chen, Multiple ground-state instabilities in the anisotropic quantum Rabi model, *Phys. Rev. A* **103**, 043708 (2021).
- [74] G. Zhang and H. Zhu, Analytical solution for the anisotropic Rabi model: effects of counter-rotating terms, *Sci. Rep.* **5**, 8756 (2015).
- [75] Y.-Y. Zhang, Generalized squeezing rotating-wave approximation to the isotropic and anisotropic Rabi model in the ultrastrong-coupling regime, *Phys. Rev. A* **94**, 063824 (2016).
- [76] Z. H. Wang, Q. Zheng, X. Wang, and Y. Li, The energy-level crossing behavior and quantum Fisher information in a quantum well with spin-orbit coupling, *Sci. Rep.* **6**, 22347 (2016).
- [77] A. L. Grimsmo and S. Parkins, Cavity-QED simulation of qubit-oscillator dynamics in the ultrastrong-coupling regime, *Phys. Rev. A* **87**, 033814 (2013).
- [78] L.-B. Fan, Y.-H. Zhou, F. Zou, H. Guo, J.-F. Huang, and J.-Q. Liao, Quantum thermalization and vanishing

- thermal entanglement in the open Jaynes–Cummings model, *Ann. Phys. (Berlin)* **532**, 2000134 (2020).
- [79] W.-Y. Liu, L.-B. Fan, Y.-X. Zeng, J.-F. Huang, and J.-Q. Liao, Quantum thermalization and thermal entanglement in the open quantum Rabi model, *Ann. Phys. (Berlin)* **535**, 2200502 (2023).
- [80] A. F. Kockum, A. Miranowicz, S. De Liberato, S. Savasta, and F. Nori, Ultrastrong coupling between light and matter, *Nat. Rev. Phys.* **1**, 19 (2019).
- [81] H. P. Breuer and F. Petruccione, *The Theory of Open Quantum Systems* (Oxford University Press, Oxford, 2002).
- [82] M. Scala, B. Militello, A. Messina, J. Piilo, and S. Maniscalco, Microscopic derivation of the Jaynes-Cummings model with cavity losses, *Phys. Rev. A* **75**, 013811 (2007).
- [83] V. Montenegro and M. Orszag, Creation of entanglement of two atoms coupled to two distant cavities with losses, *J. Phys. B: At. Mol. Opt. Phys.* **44**, 154019 (2011).
- [84] G. McCauley, B. Cruikshank, D. I. Bondar, and K. Jacobs, Accurate Lindblad-form master equation for weakly damped quantum systems across all regimes, *npj Quantum Inf.* **6**, 74 (2020).
- [85] F. Minganti, A. Biella, N. Bartolo, and C. Ciuti, Spectral theory of Liouvillians for dissipative phase transitions, *Phys. Rev. A* **98**, 042118 (2018).
- [86] T. Mori and T. Shirai, Symmetrized Liouvillian gap in Markovian open quantum systems, *Phys. Rev. Lett.* **130**, 230404 (2023).
- [87] H. Carmichael, *Statistical Methods in Quantum Optics 1: Master Equations and Fokker-Planck Equations* (Springer, New York, 1999).
- [88] H. J. Carmichael, *Statistical Methods in Quantum Optics 2: Non-classical Fields* (Springer, New York, 2009).
- [89] R. J. Glauber, Nobel lecture: One hundred years of light quanta, *Rev. Mod. Phys.* **78**, 1267 (2006).
- [90] R. J. Glauber, The quantum theory of optical coherence, *Phys. Rev.* **130**, 2529 (1963).
- [91] P. Rabl, Photon blockade effect in optomechanical systems, *Phys. Rev. Lett.* **107**, 063601 (2011).
- [92] A. Ridolfo, M. Leib, S. Savasta, and M. J. Hartmann, Photon blockade in the ultrastrong coupling regime, *Phys. Rev. Lett.* **109**, 193602 (2012).
- [93] L. Garziano, A. Ridolfo, R. Stassi, O. Di Stefano, and S. Savasta, Switching on and off of ultrastrong light-matter interaction: Photon statistics of quantum vacuum radiation, *Phys. Rev. A* **88**, 063829 (2013).
- [94] A. Lukš, V. Peřinová, and J. Peřina, Principal squeezing of vacuum fluctuations, *Opt. Commun.* **67**, 149 (1988).
- [95] R. Stassi, S. Savasta, L. Garziano, B. Spagnolo, and F. Nori, Output field-quadrature measurements and squeezing in ultrastrong cavity-QED, *New J. Phys.* **18**, 123005 (2016).
- [96] C. Noh and H. Nha, Output field squeezing in a weakly-driven dissipative quantum Rabi model, *Opt. Commun.* **435**, 350 (2019).
- [97] C.-W. Lee and H. Jeong, Quantification of macroscopic quantum superpositions within phase space, *Phys. Rev. Lett.* **106**, 220401 (2011).
- [98] J. Eisert and M. B. Plenio, A comparison of entanglement measures, *J. Mod. Opt.* **46**, 145 (1999).
- [99] K. Życzkowski, P. Horodecki, A. Sanpera, and M. Lewenstein, Volume of the set of separable states, *Phys. Rev. A* **58**, 883 (1998).
- [100] M. B. Plenio, Logarithmic negativity: a full entanglement monotone that is not convex, *Phys. Rev. Lett.* **95**, 090503 (2005).
- [101] J. Lee, M. S. Kim, Y. J. Park, and S. Lee, Partial teleportation of entanglement in a noisy environment, *J. Mod. Opt.* **47**, 2151 (2000).
- [102] G. Vidal and R. F. Werner, Computable measure of entanglement, *Phys. Rev. A* **65**, 032314 (2002).
- [103] H. Ollivier and W. H. Zurek, Quantum discord: a measure of the quantumness of correlations, *Phys. Rev. Lett.* **88**, 017901 (2001).
- [104] S. Luo, Quantum discord for two-qubit systems, *Phys. Rev. A* **77**, 042303 (2008).
- [105] M. Ali, A. R. P. Rau, and G. Alber, Quantum discord for two-qubit X states, *Phys. Rev. A* **81**, 042105 (2010); **82**, 069902(E) (2010).
- [106] H.-G. Xu, C. Wang, and X.-L. Gao, Two-photon statistics of nonclassical radiation in the dissipative finite-size Dicke model, *J. Phys. B: At. Mol. Opt. Phys.* **53**, 155406 (2020).